DECORATION OF SPECIFIC SITES ON FREEZE-FRACTURED MEMBRANES

HEINZ GROSS, OLAF KUEBLER, ENIS BAS, and HANS MOOR

From the Institut für Zellbiologie, and the Institut für Technische Physik, Eidgenössische Technische Hochschule, Hönggerberg, CH-8093 Zürich, Switzerland

ABSTRACT

Fracturing under ultrahigh vacuum (UHV, $P \leq 10^{-9}$ Torr) produces membrane fracture faces devoid of contamination. Such clean surfaces are a prerequisite for studies of interactions between condensing gases and distinct regions of a surface.

For the study of water condensation, a device has been developed which enables production of pure water vapor and controlled variation of its partial pressure in an UHV freeze-fracture apparatus.

Experiments with yeast plasmalemma fracture faces, produced at −196°C and exposed to pure water vapor before replication, resulted in a "specific decoration" with ice crystals of those pits in the extraplasmic face where the corresponding particles of the plasmic face had been removed. Because water condenses as discrete ice crystals which resemble intramembrane particles, ice crystals might easily be misinterpreted as actual membrane structures. At low specimen temperature ($T \leq -110$°C) the structural features of membrane fracture faces produced under high vacuum ($P \sim 10^{-6}$ Torr) should, therefore, be interpreted with caution.

KEY WORDS UHV freeze-fracturing membrane structure baker's yeast contamination specific condensation patterns particle-like ice crystals

A characteristic feature of freeze-fractured biological specimens is membrane cleavage, which leads to the visualization of the so-called intramembrane particles (1, 2, 8, 11). If the structural details of both fracture faces produced by the cleavage are compared, a certain lack of complementarity is usually observed. In the yeast plasmalemma, for example, hexagonally arranged particles were found on the plasmic fracture face (*P* face), although no corresponding depressions were detectable on the extraplasmic face (*E* face) (6, 8). Progress was achieved through the application of ultrahigh vacuum UHV, ($P \leq 10^{-9}$ Torr) and very low specimen temperature (−196°C), as demonstrated by the presence of ordered regions with complementary details on both fracture faces of the yeast plasmalemma (6, 7). Through the use of digital image processing, the corresponding structures were shown to fit together with an accuracy of 20 Å (7). The improvement attained with the new technique could be explained by reduced structural distortion (plastic deformation) during fracturing at lower specimen temperature. UHV conditions were necessary only to keep the fracture faces clean.

Under conventional vacuum conditions ($\sim 10^{-6}$ Torr), low temperature surfaces ($T \leq -110$°C) become contaminated (4, 8, 10). Contamination is mainly caused by the condensation of water vapor, which is the major residual gas in conventional high vacuum systems (6, 8). With fractured

J. CELL BIOLOGY © The Rockefeller University Press · 0021-9525/78/1201-0646$1.00
Volume 79 December 1978 646-656

lipid-water and glycerol-water mixtures, Deamer et al. (4), and Staehelin and Bertaud (10) have shown that the deposition of residual gases not only hides the actual structures but also creates artificial ones resembling intramembrane particles. This substrate-specific contamination pattern, caused by a nonrandom distribution of the condensate, revealed the possibility of the use of condensing materials as labels for regions on the fracture faces with certain physicochemical properties.

For a better understanding of such "decoration" phenomena, some physical aspects of the condensation process must be considered (3, 12). When an atom or molecule impinges on a substrate, it must lose at least the energy associated with its motion normal to the substrate in order to be adsorbed on the surface. Equilibration with the substrate is achieved by dissipation of the energy of condensation. An atom which has, after collision, an energy higher than the activation energy necessary for surface diffusion is free to migrate over the surface. Even if an atom has reached equilibrium with the surface, it is still free to change its place by surface diffusion. Statistically, this energy is supplied from the substrate. The adsorbed atom has a finite "lifetime" before it reevaporates. During this time it may collide with other migrating atoms and form a nucleus of more than one atom. Some of these nuclei will grow and form clusters of critical size, that is, stable nuclei that, once formed, grow very rapidly at the expense of subcritical clusters and single adsorbed atoms. Finally, the nuclei will coalesce into a continuous film.

These aspects show that surface movement provides the condition necessary for the formation of discrete, particulate structures in the condensate: If the condensing vapor atoms are laterally displaceable on the surface, and if the exposed structures cause an unequal distribution of surface forces, the migrating atoms or molecules will be able to settle at places with high binding energy where their "lifetime" is extended, therefore making the formation of stable nuclei more probable.

Studies of interactions between distinct condensing materials and certain physicochemically-defined regions on a fracture face require a surface devoid of unknown contamination. At a pressure of 10^{-6} Torr it takes only about 1 s for exposed surfaces to be covered with a monomolecular contamination layer (assuming homogeneous distribution). Investigations of the interactions between decorating materials and a surface, especially at very low temperature, are therefore only possible if the fracture face is produced under UHV conditions.

First experiments were carried out by exposing membrane fracture faces to pure water vapor. For this, a device was developed which allows both the production of pure water vapor and the controlled variation of its partial pressure inside the bell jar of an UHV freeze-fracture apparatus. In this paper, it is shown that the condensation pattern of water produces decoration phenomena which can be correlated with the architecture of the exposed membrane fracture faces. Furthermore, the formation of condensate crystals that resemble intramembrane particles is demonstrated.

MATERIALS AND METHODS

Production of Pure Water Vapor

A schematic outline of the device for generation and storage of pure water vapor is shown in Fig. 1 *a*. Under vacuum ($P \leq 10^{-3}$ Torr), a small container (1) filled with copper-sulfate-pentahydrate (≥99%, Fluka A. G., Buchs, Switzerland) is heated to 100°C with a heating coil (2), with the temperature controlled by means of a thermocouple (3). The water of hydration thereby released enters a large storage vessel (6). From there, water vapor is released through a connection tube (7) and a gas-dosing and gas-inlet valve (8) into the bell jar of the UHV freeze-fracture apparatus.

Mass spectra (Figs. 1 *b*, *c*) show that the purity of the released water vapor is at least 99% (background vacuum 1×10^{-9} Torr). Except for peak 28, representing nitrogen or carbon monoxide, all other peaks originate from water.

Specimen Preparation

The interpretation of decoration phenomena is greatly facilitated if methods of image averaging (i.e., optical diffraction, digital Fourier filtration, and reconstruction of filtered data) can be applied. The plasmalemma of baker's yeast, which contains a paracrystalline structure, was therefore chosen as test specimen. Pressed yeast cells from a local yeast supplier were suspended in distilled water and stored at room temperature for 24 h. Then the suspension was gently spun down, and several small brass capillaries (specimen holders [5, 6]) were filled with the pelleted cells. The highly concentrated cell suspensions were frozen in liquid Freon-22 at −160°C.

Decoration Experiments and Electron Microscopy

Three capillaries immersed in liquid nitrogen were

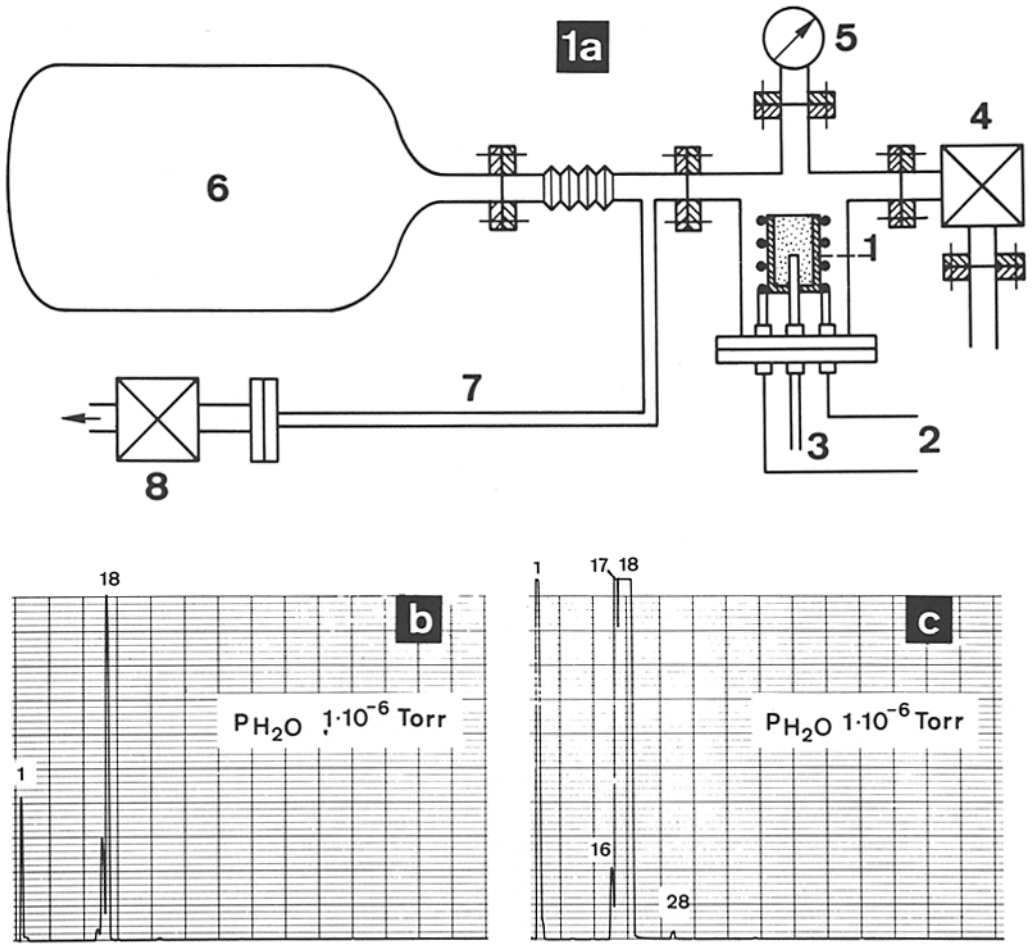

FIGURE 1 Production of pure water vapor. (*a*) Schematic outline of the device: (1) ceramic container filled with copper-sulfate-pentahydrate (0.5 gm); (2) heating-coil; (3) thermocouple; (4) vacuum valve; (5) vacuum gauge; (6) storage vessel; (7) connection to the UHV bell jar; (8) UHV inlet-valve. (*b, c*) Mass spectrograms recorded inside the UHV bell jar during introduction of water (background vacuum 1×10^{-9} Torr).

fixed in the specimen cartridge and transferred into the airlock of the UHV freeze-fracture apparatus. Hoar-frost formation was prevented by transferring the cartridge to the airlock under liquid nitrogen and by venting the pre-evacuated airlock with dry nitrogen gas. After pump-down of the airlock, the cartridge was transferred to the ultrahigh evacuated bell jar and inserted into the pre-cooled specimen stage. Once the cartridge had been placed in the stage, ultrahigh vacuum ($P \leq 10^{-9}$ Torr) was re-established within ~1 h (details in [5, 6]).

To achieve precise and reproducible control of the exposure to pure water vapor the required partial pressure of water was established before the fracture faces were produced. At a residual gas pressure of $P \leq 1 \times 10^{-9}$ Torr, the inlet-valve for water vapor was opened and regulated until the required equilibration pressure was attained. Fracturing was then performed at −196°C by advancing a liquid nitrogen-cooled plate over the cartridge. The capillaries were successively broken at the predetermined zones, and the resulting fracture faces exposed to water vapor. Then the inlet-valve was closed, which caused immediate return to UHV conditions ($P \leq 3 \times 10^{-9}$ Torr, attained within 1–2 s). Further interaction between released gas and the specimen surface was thus prevented. Subsequent coating was performed by Pt/C-shadowing and C-backing (details in [5, 6]). After coating, the specimens were withdrawn through the airlock and thawed. The replicas were floated on 25% aqueous CrO_3 overnight, then washed several times in double-distilled water and mounted on naked grids (400 mesh). The replicas were examined in a Siemens 102 electron microscope, equipped with an

anticontamination device, at a beam voltage of 100 kV and at × 50,000. Pictures were taken on Agfa-Gevaert Scientia plates (Dübendorf, Switzerland). Magnifications were calibrated with a cross-grating (54,800 lines/inch, Balzers-Union, Liechtenstein). The negatives were used directly for producing enlarged positives (shadows white).

Selection of Periodic Components and Digital Image Processing

The micrographs were selected by light-optical diffraction. The position and the extent of the ordered region were marked, and the diffraction pattern was recorded on 35-mm film. The best regions with respect to both the order and the sharpness of the discrete reflexes were digitized with a raster size of (25 μm)^2 on an Optronics P-1700 photoscan/photowrite unit (Optronics International, Inc., Chelmsford, Mass.). Fourier transforms of 256 × 256 picture elements were computed. Concentrations of high intensities were located by a peak-detection routine, and their center-of-gravity positions were displayed on the line printer in a geometrical arrangement subsequently used for indexing the diffraction pattern. Reciprocal lattice vectors were obtained from a least squares fit. Only those lattices for which all experimental reflexes were in agreement with the ideal positions to within 2% of the lengths of the reciprocal vectors were retained for further processing. The Fourier filtration was done so as to give a spatial averaging of a range equal to the circular cutout of the original. The digital diffraction pattern and the processed image were displayed on the photowrite (details in [7]).

RESULTS

The structural record after UHV freeze-fracturing at very low specimen temperature (−196°C) without additional water vapor condensation (control) is shown in Figs. 2*a* and (*P* face) and 3*a* (*E* face). The most prominent structures of the yeast plasmalemma are the troughlike invaginations. In the flat areas between these invaginations, patches with paracrystalline structure are visible. On the *P* face, hexagonally ordered particles with a volcano-like shape are visible, and on the *E* face corresponding ring-like depressions can be seen. We have called the paracrystalline structure with 165 Å-lattice repeats the main structure or the main component (7). Complementarity of these periodic features on the two fracture faces was demonstrated by digital-image filtration (7). On the *E* face, an additional substructure is revealed (Figs. 4b_2, b_3). Each ring of the main structure is surrounded by a hexagonal arrangement of depressions which trisect the longer diagonal of the unit cell. Its complementarity is not yet proven (7).

Figs. 2*b* and *c* show two *P* faces after controlled exposure to pure water vapor. The vacuum before introduction of water vapor was 1 × 10^{-9} Torr (background vacuum), the specimen temperature −196°C, and the partial pressure of the released water vapor 1 × 10^{-6} Torr. Fig. 2*c* demonstrates that even after heavy deposition (exposure time 60 s) the volcano-like particles of the paracrystalline structure (one is encircled) can be detected. These particles are less prominent because water condensation has taken place mainly outside the areas of paracrystalline structure. This is clearly visible on the *P* face which was exposed for a shorter time (20 s, Fig. 2*b*). The structural features inside the paracrystalline regions (one is encircled) are similar to those of the UHV experiments without additional exposure to water vapor (Fig. 2*a*), suggesting that practically no water condensation occurs inside these regions.

The structural alterations on the *E* face caused by pure water vapor condensation are shown in Figs. 3*b*, *c*. The partial pressure of the released water vapor was again 1 × 10^{-6} Torr, and the exposure times were 5 s (Fig. 3*b*) and 60 s (Fig. 3*c*). Equal distribution and total condensation of all theoretically impinged water molecules would have resulted in 60 monomolecular layers of condensate in Fig. 3*c* and 5 layers in 3*b*. After exposure to water vapor for 5 s, the patches with regularly arranged ring-like depressions appear with about the same distinctness (Fig. 3*b*) as in UHV experiments in which additional water was not introduced (Fig. 3*a*). The only indications of water condensation are some particulate structures (arrows) which have primarily formed inside the paracrystalline regions. On the *E* face exposed for 60 s, all topographic details of the depressions are hidden (Fig. 3*c*). But the location of the paracrystalline regions (two are encircled) can be recognized because particulate structures have formed in patches of the same size and location. Discrete ice crystals with an angular shape can be recognized in these patches; this demonstrates that on the *E* face, also, water does not condense uniformly as a homogeneous layer.

At higher magnification (Fig. 4*a*) two observations can be made. First, the ice crystals have a cubic shape (arrow) and an edge length of about 60 Å. Second, they seem to be regularly arranged. In the row labeled with asterisks the uniform distance between ice crystals is evident. This implies that the lattice of the underlying depressions is reflected in the arrangement of the ice crystals

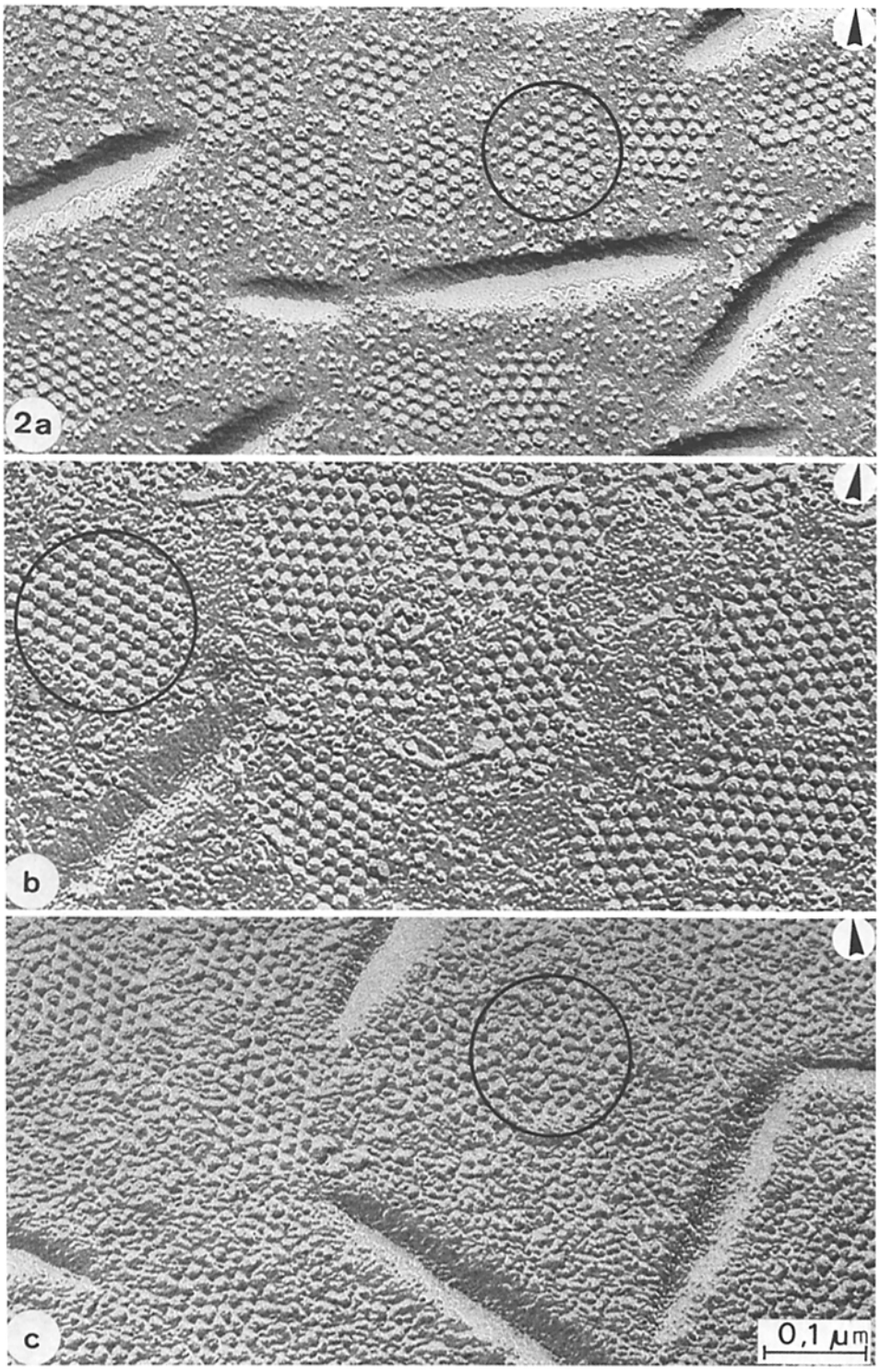

FIGURE 2 Plasmic fracture faces of yeast plasmalemma, freeze-fractured at −196°C and Pt/C-shadowed at $P \leq 3 \times 10^{-8}$ Torr. (*a*) Replicated immediately after fracturing (control). (*b*, *c*) Before replication, exposed for (*b*) 20 s and (*c*) 60 s to pure water vapor (partial pressure 1×10^{-6} Torr). The micrographs demonstrate that the volcano-like particles in the paracrystalline structure (encircled) can still be detected after water deposition. The particles appear less prominent because water condensation has taken place mainly outside these regions. Arrows indicate direction of shadowing. × 150,000.

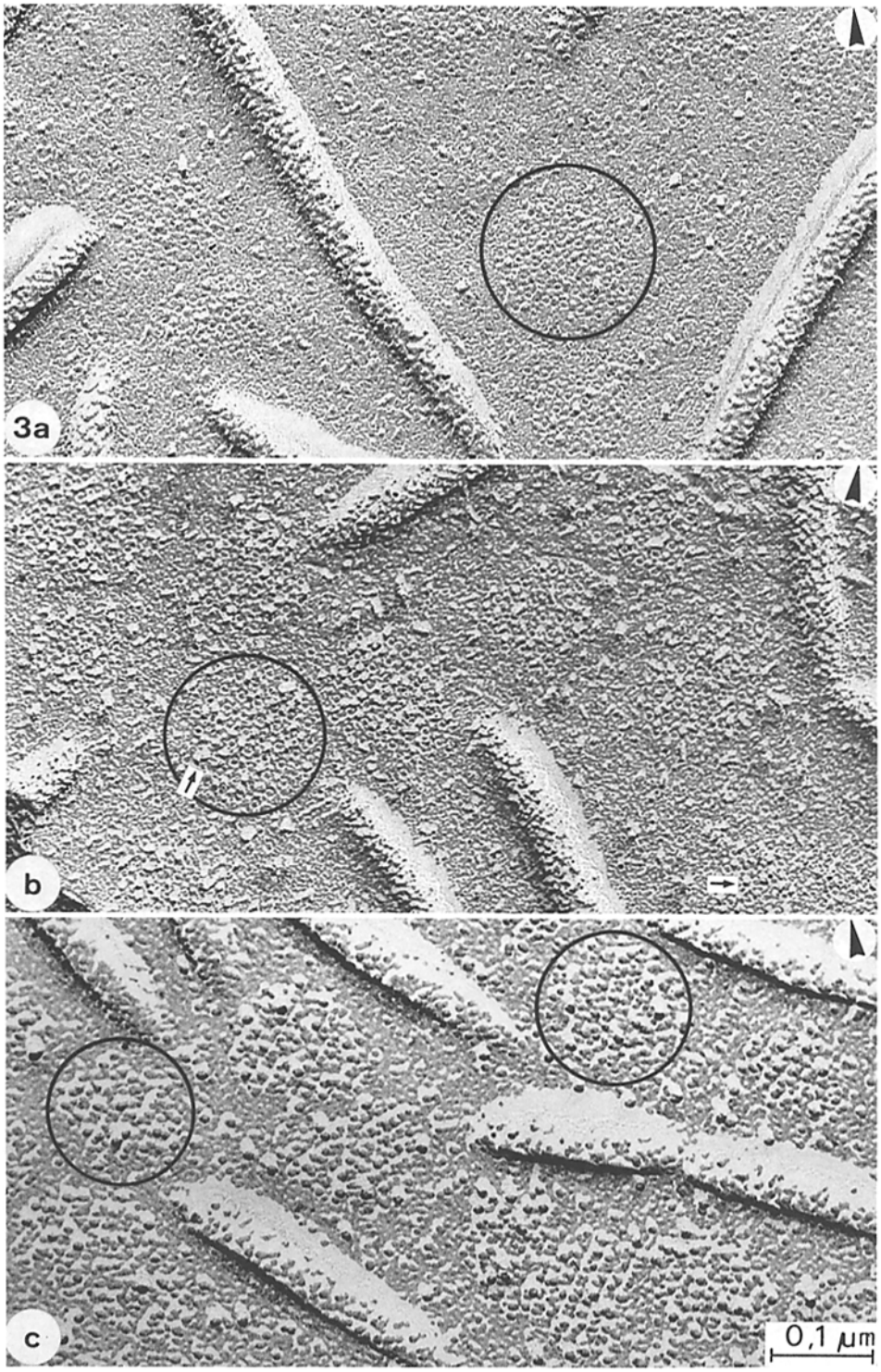

FIGURE 3 Extraplasmic fracture faces of yeast plasmalemma, freeze-fractured at −196°C and Pt/C-shadowed at P ≤ 3 × 10^{-9} Torr. (*a*) Replicated immediately after fracturing (control). (*b, c*) Before replication, exposed for (*b*) 5 s and (*c*) 60 s to pure water vapor (partial pressure 1 × 10^{-6} Torr). The micrographs demonstrate that on the *E* face, water does not condense uniformly as a homogeneous layer. In contrast to the *P* face, ice crystals have mainly formed in the patches with paracrystalline structure (encircled). On the *E* face, exposed for only 5 s, small ice crystals which resemble intramembrane particles (arrows), as well as nonhidden depressions, can be recognized. Arrows indicate directions of shadowing. × 150,000.

("specific decoration"). This assumption can be verified by the use of digital image processing (which filters out the random noise). The lower part of Fig. 4 shows three paracrystalline regions before (upper row) and after (middle row) Fourier filtration. The filtered image after UHV freeze-fracturing at −196°C without additional water condensation (Fig. $4b_2$) reveals the ringlike depressions of the main structure (two concentric circles in Fig. $4b_3$), with 165 Å lattice repeats and the surrounding pits (substructure), also hexagonally arranged (simple circles in Fig. $4b_3$). The filtered images of the two patches replicated after controlled water condensation at different impingement rates (different partial pressures of the released water vapor) show that at the higher impingement rate ($pH_2O = 10^{-5}$ Torr, Fig. $4c_2$) the ring-like depressions of the main structure are predominantly decorated with discrete ice crystals, while at the lower rate ($pH_2O = 10^{-7}$ Torr, Fig. $4d_2$) ice crystals tend to grow selectively in the pits surrounding the ring-like depressions.

The appearance of the deposition pattern of condensed water molecules can be influenced not only by the incident water flux but also by additional, simultaneously impinging, gas molecules, Fig. 5 shows yeast cells with both fracture faces of the plasmalemma exposed. The specimens were fractured at −196°C and, before replication, exposed for 60 s to a vacuum of 1×10^{-6} Torr with a residual gas composition of about 60% nitrogen and 30% water vapor, hydrogen, and carbon dioxide. Large cubic ice crystals with an edge length of at least 1,000 Å were formed mainly on the *E* faces, while the *P* faces are predominantly covered by smaller ice crystals. On the surface of the ice, between the cells, the deposit is so compact that no trace of condensate structure can be detected. Total condensation of all theoretically impinged water molecules (partial pressure of water $\sim 3 \times 10^{-7}$ Torr) and equal distribution on the surface would have resulted in a homogeneous layer of deposition of ~50 Å. The formation of large ice crystals, instead, indicates a very high lateral mobility (surface diffusion) of the condensing water molecules on membrane fracture faces.

DISCUSSION

Freeze-fracturing under UHV conditions with and without exposure to pure water vapor, the major residual gas in conventional high vacuum systems (6, 8), allows identification of structural alterations introduced by condensing water molecules (main contamination). The UHV experiments without additional water condensation showed hexagonally arranged depressions on the *E* face that were practically devoid of particulate structural features (6, 7), (Fig. $3a$). When the amount of released water vapor was increased, the number of ice crystals grew and reached a density at which all depressions were covered and consequently all topographic details were hidden. The actual uncontaminated structure of the paracrystalline regions on the *E* face seems therefore to consist of depressions without any particulate structure. Both the appearance of water condensation as discrete, particle-like ice crystals, and their preferred formation on the depression, opposite to the corresponding actual particles, may easily lead to misinterpretation of ice crystals as membrane structures. Therefore, the structural features of membrane fracture faces produced under high vacuum conditions ($P \sim 10^{-6}$ Torr), especially at low specimen temperature ($T \leq -110$°C), or produced while immersed in liquid gases (nitro-

FIGURE 4 (*a*) Extraplasmic fracture face of the yeast plasmalemma after exposure (60 s) to pure water vapor (1×10^{-6} Torr). At higher magnification (× 400,000) the cubic shape of the ice crystals becomes visible (arrow). In the row labeled with asterisks the uniform distance between ice crystals can be recognized. (*b–d*) Three paracrystalline regions of the *E* face, with and without superimposed ice crystals, are shown before ($b_1 - d_1$) and after ($b^2 - d_2$) Fourier filtration. The filtered image of a specimen after UHV freeze-fracturing at −196°C without additional water condensation (b_2) reveals the ring-like depressions of the main structure (two concentric circles in diagram b_3) and the depressions of the substructure (simple circles in diagram b_3). The filtered images of specimens which have been exposed to different partial pressures of water vapor, demonstrate that at the higher impingement rate ($pH_2O = 10^{-5}$ Torr) it is the main structure (c_2, black spots in diagram c_3) which is predominantly decorated with ice crystals, but at the lower rate ($pH_2O = 10^{-7}$ Torr) it is the substructure (d_2, black spots in diagram d_3), which is predominantly ice-crystal decorated. Arrows indicate direction of shadowing. Bar represents 500 Å (× 300,000).

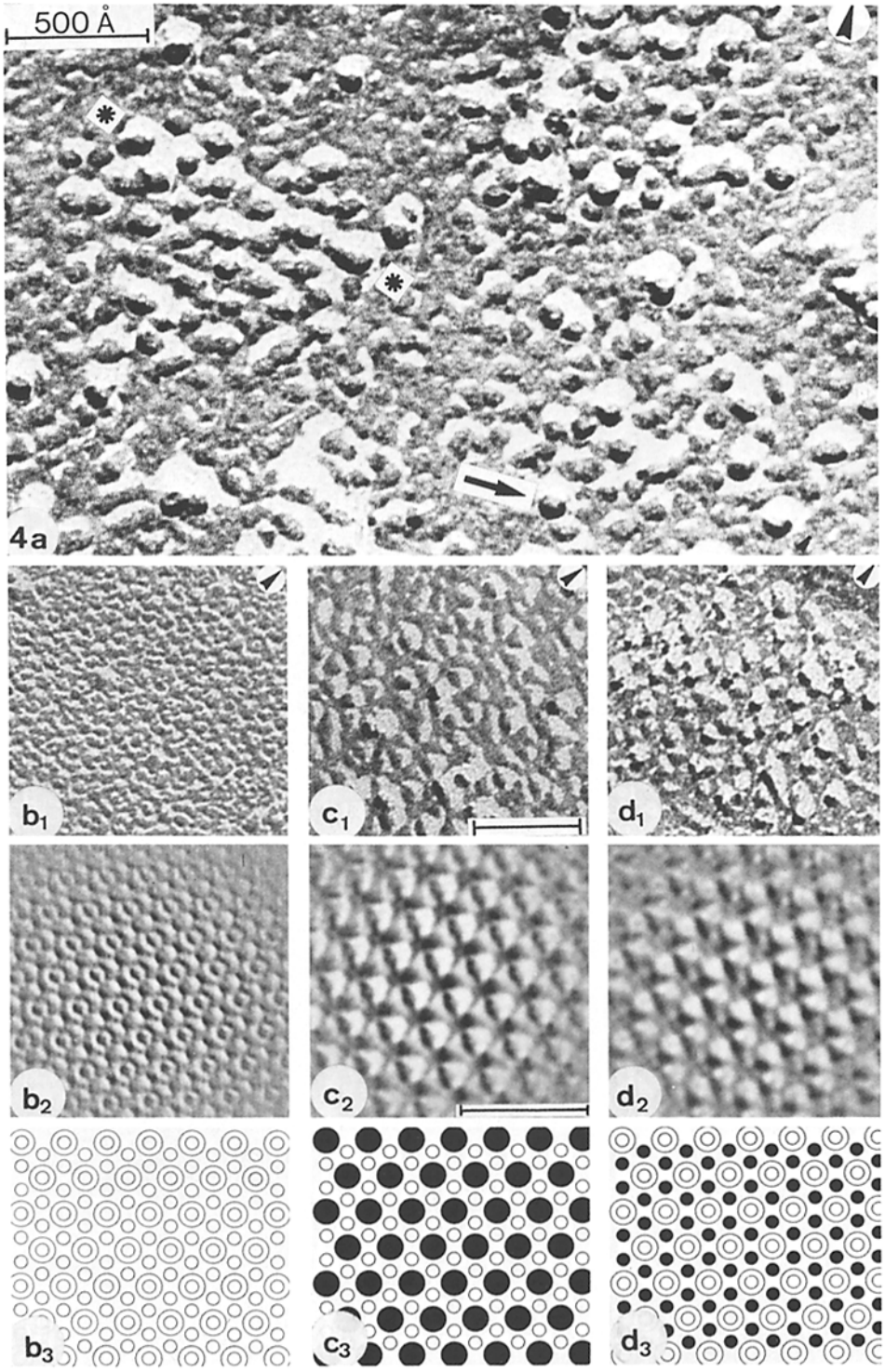
500 Å
4a
b1
c1
d1
b2
c2
d2
b3
c3
d3

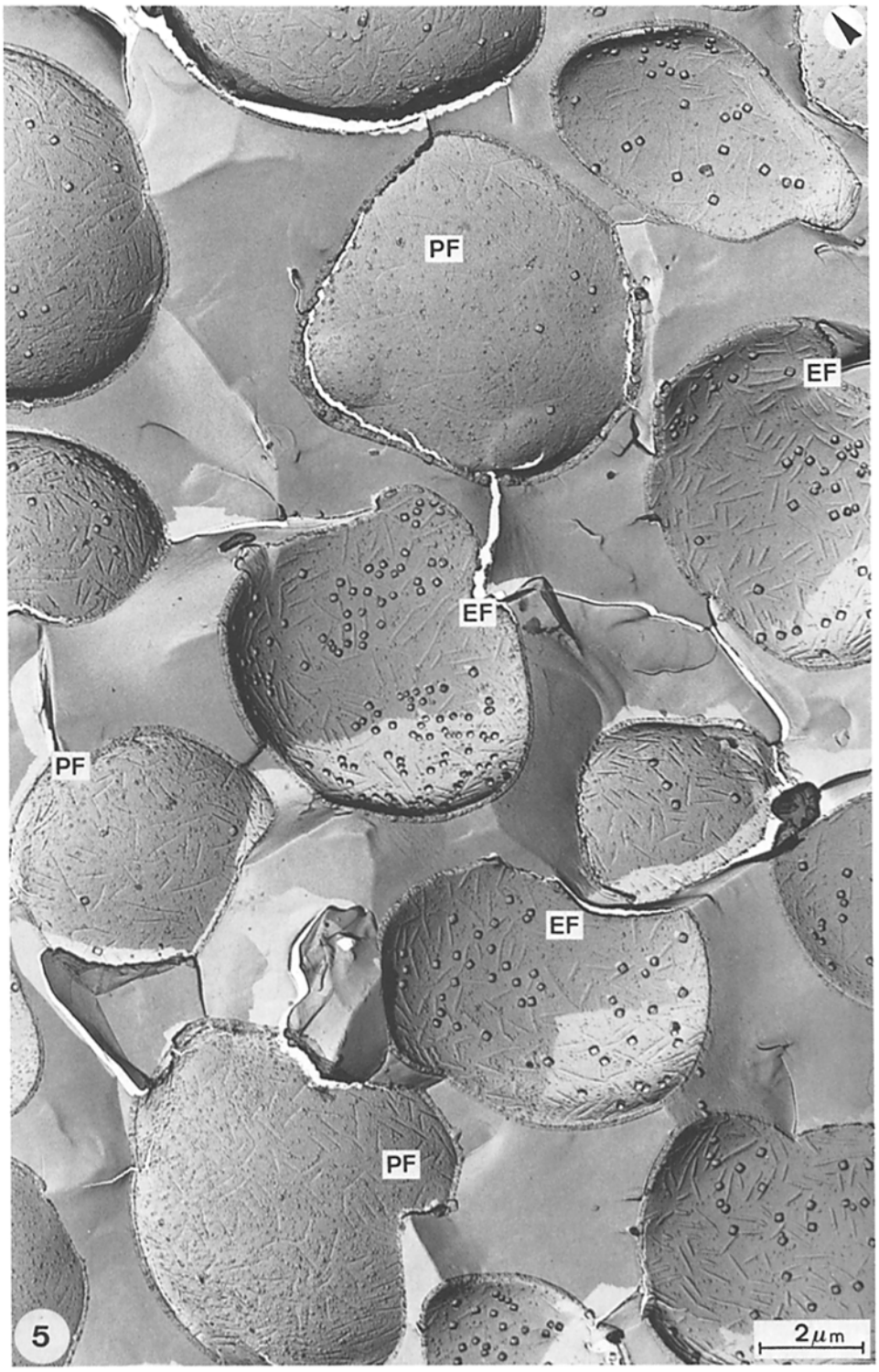

FIGURE 5 Yeast cells which exhibit both fracture faces of the yeast plasmalemma. These specimens were fractured at −196°C and exposed for 60 s to a vacuum of 1×10^{-6} Torr with a high content of nitrogen (~60%) and only ~30% water vapor before replication. The appearance of large cubic ice crystals with an edge length of at least 1,000 Å (mainly formed on the *E* faces) indicates that the deposition pattern of condensed water vapor can be influenced by additional, simultaneously impinging, gas molecules. Arrow indicates direction of shadowing. × 7,500.

gen, helium) involving transfer into an evaporation unit, have to be interpreted with caution (e.g., Fig. 13 in reference 2 and Figs. 9, 10 in reference 9).

The appearance of water condensation as discrete particulate structures even at very low specimen temperatures (−196°C) disproves, moreover, of the widely-held opinion that portrayal of holes in membrane fracture faces is indicative of a contamination-free replication. On the *E* face exposed for 5 s (partial pressure of water 1×10^{-6} Torr, theoretically 5 monomolecular layers), both small ice crystals and nonhidden ring-like depressions can be recognized (Fig. 3*b*).

It must be pointed out that even in pictures obtained with UHV freeze-fracturing, occasionally cubic ice crystals can be observed (Fig. 3*a*). A possible source of the water molecules which form ice crystals even under UHV conditions may be the small outburst of water vapor observed during fracturing which causes a brief ($t \leq 1$ s) and slight ($P < 1 \times 10^{-7}$ Torr) pressure rise (6). We are currently engaged in clarifying this problem. A better understanding of sources of contamination, and their subsequent elimination, are essential for improving freeze-etching under conventional high vacuum conditions ($P \sim 10^{-6}$ Torr), also. It must be pointed out that in such systems there exist further sources of contamination. In addition to the residual gases inside the vacuum chamber, hoar-frost formation on the specimen and its surroundings, and gas production by the coating procedure must be taken into account. In our UHV device all of these sources are eliminated (5, 6). It is clear, therefore, that the usual techniques by which contamination is limited at P $\sim 10^{-6}$ Torr, such as shadowing and carbon-backing immediately after fracture, or protection of the fracture face with the cutter, may not be sufficient to provide clean images.

The formation of discrete ice crystals with a cubic shape requires lateral mobility (surface diffusion) of the condensing water molecules. The preferred formation of these ice crystals on the *E* face depressions, which reflects their hexagonally ordered arrangements ("specific decoration"), must be caused by a higher binding energy on the surface of these structures than on the surfaces of the surrounding areas. Lower binding energy means facilitated surface diffusion and desorption of subcritical nuclei and single molecules, which results in a lower probability that nuclei of critical size are formed. The preferred growth of ice crystals on these structures could be caused by the cavity-like character of their curved surface or by polar surface properties. The high lateral mobility of the condensing water molecules observed in the presence of a considerable amount of nitrogen (Fig. 5), and the fact that the craters of the *P* face particles with similar curved surfaces do not act as nucleation sites, indicate that the polar surface properties and not the geometrical shape, cause the trapping of the water molecules in the regions of the depressions.

Besides the physicochemical properties of the underlying substrate, the substrate temperature and the number of molecules adsorbed on the surface per unit time (directly proportional to the impingement rate) determine the form of condensation products. The fewer the adsorbed water molecules, the lower the probability of nucleation. On a substrate with different exposed structures that cause an unequal distribution of surface forces, the impinging molecules will be able to settle at places with high binding energy, where their "lifetime" is extended and, therefore, the formation of stable nuclei will be more probable. The preferred growth of ice crystals on the pits surrounding the ring-like depressions (Fig. 4*d*) at lower impingement rates (partial pressure of water $\sim 10^{-7}$ Torr) implies, therefore, higher binding energy in these regions compared to the ring-like depressions themselves. At higher impingement rates (partial pressure of water $\sim 10^{-5}$ Torr, Fig. 4*c*), the density of adsorbed water molecules on the surface seems to be so high that nucleation on both structures is probable. But in the ring-like depressions ice crystal growth seems to be more rapid, which leads to prominent crystals mainly on these structures. Precise inspection of the filtered image (Fig. $4c_2$) reveals, however, small ice crystals over the pits as well.

The pattern of water condensation is altered either by a change in the incident flux of the water molecules themselves or by the introduction of simultaneously-impinging nitrogen molecules; this demonstrates the sensitivity of such decoration experiments even on complex membrane fracture faces. At −196°C, the saturation vapor pressure of nitrogen is still so high (~1,000 Torr) that no nitrogen condensation can have taken place. A gas can condense only if it is in the supersaturated state, i.e., if its partial pressure is greater than its saturation vapor pressure at the temperature of the substrate. Molecules of a gas can, however, adsorb to the substrate even in the unsaturated

condition (covering the surface with at least one monomolecular layer). Adsorbed nitrogen molecules may therefore be responsible for the different condensation behaviour of water vapor when nitrogen is present in the incident beam flux.

The observations that the *P*-face particles of the main structure are elevated by at least 40 Å, that these are almost perfectly matched by *E* face depressions, as described before (7), and that the depressions are obviously decorated with ice crystals at higher impingement rates, together support the assumption that the particles penetrate the outer half of the yeast plasmalemma and reach the outer membrane surface. It is therefore not unlikely that, in the depressions, the outer leaflet of the lipid bilayer is interrupted and that a surface area with polar properties is exposed. Such a surface would be characterized by a high binding energy to polar water molecules and hence by a high probability for nucleation and ice crystal growth. Outside of the depressions, where the apolar chains of the outer leaflet are exposed, the interaction with the impinging water molecules seems to be so weak that even at very low specimen temperature (−196°C) the trapped water molecules diffuse to the periodic structures or even desorb. This interpretation is supported by the fact that the corresponding particles remain visible even after heavy water deposition (Fig. 2*c*). The weak interaction with polar water molecules is in harmony with the expected hydrophobic properties of intrinsic membrane particles.

We are aware that this is a speculative interpretation which must be confirmed with the help of simple model systems. However, these initial experiments show that with controlled deposition of suitable condensing gases on clean surfaces, "specific decoration" is possible even at very low specimen temperature and, therefore, can be used in combination with UHV freeze-fracturing to label regions with certain physicochemical properties on membrane fracture faces. Such investigations may be useful in overcoming one of the most serious limitations of freeze-fracturing: the lack of chemical information in the replicas.

We thank Miss D. Walzthöny and Mr. A. Frey for their excellent technical assistance, and Dr. D. Turner for his critical reading of this manuscript and the help with English.

This research was supported by the Swiss National Science Foundation, grant 3.690-0.76.

Received for publication 23 February 1978, and in revised form 7 August 1978.

REFERENCES

1. Branton, D. 1971. Freeze-etching studies of membrane structure. *Philos. Trans. R. Soc. Lond. B Biol. Sci.* **261**:133–138.
2. Bullivant, S. 1973. Freeze-etching and freeze-fracturing. *In* Advanced Techniques in Biological Electron Microscopy, J. K. Koehler, editor. Springer-Verlag KG., Berlin, Germany. 67–112.
3. Chopra, K. L. 1969. Nucleation, growth, and structure of films. *In* Thin Film Phenomena. McGraw-Hill Book Company, New York. 137–265.
4. Deamer, D. W., R. Leonard, A. Tardieu, and D. Branton. 1970. Lamellar and hexagonal lipid faces visualized by freeze-etching. *Biochim. Biophys. Acta.* **219**:47–60.
5. Gross, H. 1977. Gefrierätzung im ultrahochvakuum (UHV) bei −196°C. Dissertation 5881. Eidgenössische Technische Hochschule-Zürich, Switzerland.
6. Gross, H., E. Bas, and H. Moor. 1978. Freeze-fracturing in ultrahigh vacuum (UHV) at −196°C. *J. Cell Biol.* **76**:712–728.
7. Kuebler, O., H. Gross, and H. Moor. 1978. Complementary structures of membrane fracture faces obtained by ultrahigh vacuum freeze-fracturing at −196°C and digital image processing. *Ultramicroscopy.* **3**:161–168.
8. Moor, H. 1971. Recent progress in the freeze-etching technique. *Philos. Trans. R. Soc. Lond. B Biol. Sci.* **261**:121–131.
9. Sleytr, U. B., and A. W. Robards. 1977. Freeze-fracturing: a review of methods and results. *J. Microsc. (Oxf.).* **111**:77–100.
10. Staehelin, L. A., and W. S. Bertaud. 1971. Temperature and contamination dependent freeze-etch images of frozen water and glycerol solutions. *J. Ultrastruct. Res.* **37**:146–168.
11. Zingsheim, H. P. 1972. Membrane structure and electron microscopy. The significance of physical problems and techniques. (Freeze-etching). *Biochim. Biophys. Acta.* **265**:339–366.
12. Zinsmeister, G. 1973. Gegenwärtiger Stand der Kondensation dünner Schichten. *Vak.-Tech.* **22**:85–93.